Impact of surface roughness in nanogap plasmonic systems

Cristian Ciracì,*,† Ferran Vidal-Codina,‡ Daehan Yoo,¶ Jaime Peraire,‡

Sang-Hyun Oh,¶ and David R. Smith§

† Center for Biomolecular Nanotechnologies, Istituto Italiano di Tecnologia, Via Barsanti, 73010 Arnesano, Italy

‡Department of Aeronautics and Astronautics, Massachusetts Institute of Technology,

Cambridge, MA 02139, USA

¶Department of Electrical and Computer Engineering, University of Minnesota,

Minneapolis, MN 55455, USA

§ Center for Metamaterial and Integrated Plasmonics, Department of Electrical and
Computer Engineering, Pratt School of Engineering, Duke University, Durham, NC 27708,

USA

E-mail: cristian.ciraci@iit.it

Abstract

Recent results have shown unprecedented control over separation distances between two metallic elements hundreds of nanometers in size, underlying the effects of freeelectron nonlocal response also at mid-infrared wavelengths. Most of metallic systems however, still suffer from some degree of inhomogeneity due to fabrication-induced surface roughness. Nanoscale roughness in such systems might hinder the understanding of the role of microscopic interactions. Here we investigate the effect of surface roughness in coaxial nanoapertures resonating at mid-infrared frequencies. We show that although random roughness shifts the resonances in an unpredictable way, the impact of nonlocal effects can still be clearly observed. Roughness-induced perturbation on the peak resonance of the system shows a strong correlation with the effective gap size of the individual samples. Fluctuations due to fabrication imperfections then can be suppressed by performing measurements on structure ensembles in which averaging over a large number of samples provides a precise measure of the ideal system's optical properties.

Keywords

plasmonics, surface roughness, nonlocal response, coaxial aperture, hydrodynamic model, epsilon-near-zero mode

Plasmonics allows the confinement of light well below the diffraction limit by greatly enhancing the electric field in the vicinity of metal surfaces. In the last decade, continuous developments in nanofabrication techniques have made it possible to control the separation distance between two metallic elements to a precision of a fraction of a nanometer. ^{1–7} Such systems, generally referred to as nanogap plasmonic structures, can squeeze light down to deep sub-wavelength volumes, allowing for the optical radiation to probe sub-atomic interactions. ^{8–16} Most of metallic systems however, still suffer from some degree of inhomogeneity due to nanoscale surface roughness, ^{17–19} which results in deviations of the optical properties with respect to ideally smooth systems. ^{20,21} Recent publications have reported on the important role of surface roughness on the far- and near-field as well as nonlinear optical properties of nanoparticles. ^{22–25}

In an experiment published in 2012,²⁶ it was shown that the resonance of a film-coupled nanoparticle system undergoes a shift that cannot be explained by a simple *local* constitutive relation between the electric field \mathbf{E} and the polarization \mathbf{P} of a metal: a more complex, *non-local*,²⁷ relation accounting for electron-electron interactions had to be considered in order to

predict the observed shifts. This experiment triggered a debate in the community, with some reporting a classical behavior down to sub-nanometer gaps, 28 other suggesting the anomalous shift was simply due to the presence of roughness on the metallic film surface, 29,30 although similar shifts were observed in ultra-smooth gold films obtained using template-stripping techniques. 31 In general, however, observations beyond the classical response were reported in many independent works. $^{32-39}$ More recently, measurements on coaxial nanoapertures in the mid-infrared 40 have shown an even more consistent ($\sim 1~\mu m$) shift in the resonance compared to calculations performed within the local response approximation. This work has reinvigorated the debate on whether the cause of the shift is due to sub-atomic electron-electron nonlocal interactions or simply due to a nonlocal correlation introduced by nanoscale surface roughness. 41

In this letter, we perform numerical calculations taking into account random surface roughness. In particular, we investigate the coaxial nanoaperture system and show that the effect of including roughness is to randomly shift the peak resonance towards higher or lower frequencies. The impact of this randomness on an ensemble of systems is to broaden the resonance without however affecting the resonance center of mass.

Fabrication of coaxial nanoapertures involves four steps: 40 first, gold nanopillars are patterned via electron-beam lithography; the pillars are then coated by gap-filling insulator (Al₂O₃) using atomic layer deposition (ALD); the resulting structure is covered with gold by sputtering; finally, ion milling is used to planarize the top surface and expose the Al₂O₃-filled nanocoaxial apertures. The lithography step introduces two different kind of irregularities: a line-edge roughness (seen from the top) that prevents the apertures from being perfectly circular, and a sidewall roughness. Because of the nature of the ALD process, the gap is conformal to the sidewall irregularities. However, a fully random source for the gap roughness cannot be excluded, so that in general the gap is affected by some combination of both types of irregularities. For clarity we have summarized all of the kinds of roughnesses in Fig. 1a.

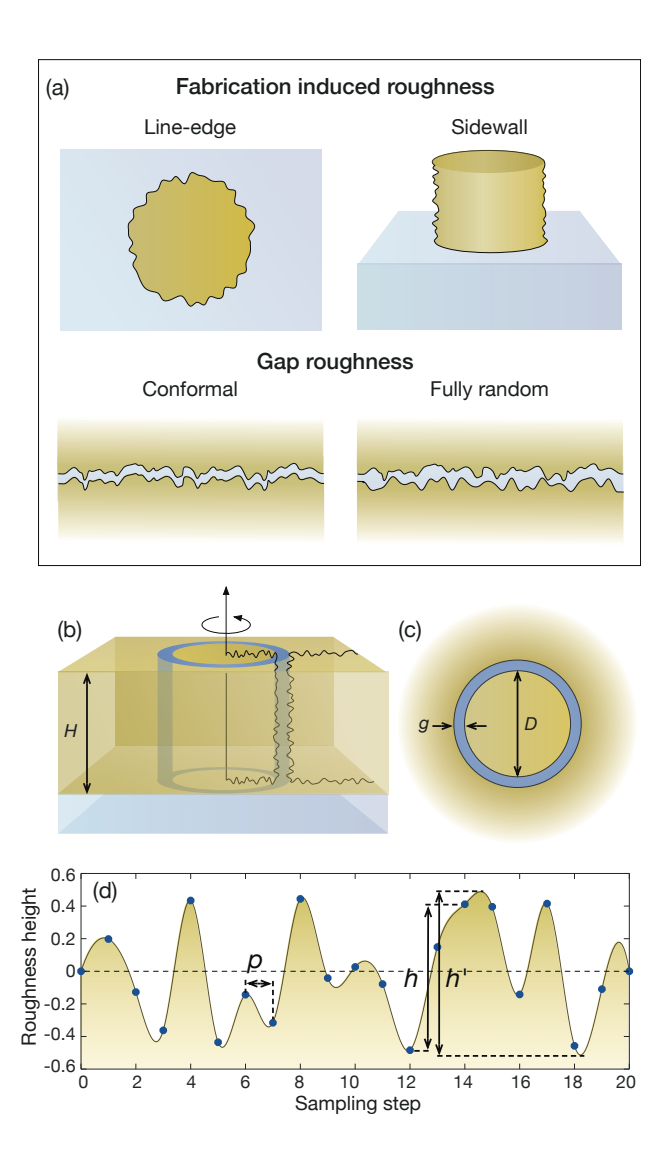


Figure 1: The coaxial nanoaperture surface roughness. In (a) a summary of the different types of roughness involved in the fabrication process. (b) shows the coaxial nanogap geometry obtained by revolving a roughnesd cross-section; the resulting top view is depicted in (c). (d) Random roughness is created using a sampling distance p and a maximum nominal height h (or effective height h').

Numerically modeling random nanoscale surface roughness can be challenging for two reasons. On one hand, it requires extended computational resources, since for example one cannot use periodic conditions and would need to discretize much more finely the computational space in order to resolve the roughness details. On the other hand, it is not straightforward creating randomness along an arbitrary surface. In order to overcome these issues, we consider isolated structures, i.e. a single annular aperture in an infinitely extended metallic film, and we solve Maxwell's equations using the so called 2.5D technique. 42,43 This technique consists in expanding all the fields in cylindrical harmonics by exploiting the axis symmetry of the geometry. In this way one needs to solve just few two-dimensional problems while still maintaining the three-dimensionality of the original one (see Methods section for more details). The drawback of this approach is that roughness can be created only in the cross-sectional plane, that is, the structure will still be smooth along the azimuthal direction as shown in Fig. 1b-c. A more general implementation could be in principle obtained by employing more complex numerical schemes that allow curvilinear elements. 44-46 Such schemes, however, go beyond the scope of this work. In this letter, we neglect line-edge roughness and consider the apertures to be perfectly circular. Moreover, because of the nature of the ALD process, we analyze irregular structures with perfectly conformal gaps or fully random gap roughness. In realistic cases, in fact, a mixture of the two type of gap roughness is expected. So, understanding the role of individual contributions is critical.

Although roughness can be readily measured on planar thin films⁴⁷ using an atomic force microscope, it is not straightforward to do the same for sidewalls of gold pillars. However, because in both cases roughness has an analogous origin we assume a roughness amplitude of the same order. Conventionally, one would use the root-mean-square (RMS) height and correlation distance to characterize a rough surface.⁴⁸ These parameters however are not ideal for generating random geometries. We use instead the following two parameters: the roughness maximum height, h', and the sampling step or average period of the roughness, p, as shown in Fig. 1d.

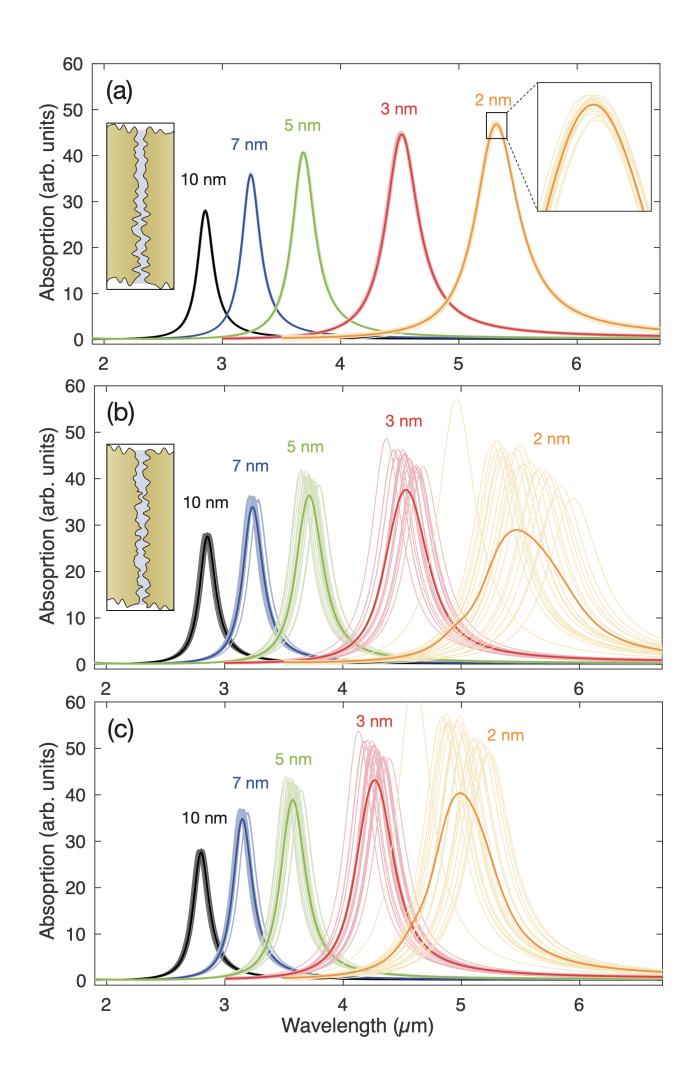


Figure 2: Absorption spectra of a single nanoring aperture for different nominal gap sizes. The light curves refers to different random roughened geometries. The thick curve is obtained by averaging all different spectra for each gap size. In (a) a conformal gap roughness, as sketched in the inset, with h = 1.8 nm ($h' \simeq 2.5$ nm) is considered. In (b) a fully random roughness, as sketched in the inset, with h = 1.4 nm ($h' \simeq 2.0$ nm) has been considered. In (c) nonlocal response effects are included for the same numerical samples as in (b).

In our 2.5D approach it is in fact possible to draw the geometry cross-section by randomly displacing each point of the curve by a distance |d| <= h/2, following steps of p, where $h \le h'$ is the nominal maximum roughness height. The displacement d of each point in the curve is independent of the displacement of their neighbors, and is drawn according to a uniform distribution, hence the roughness we prescribe exhibits no correlation length. The nominal maximum roughness values that we use are h = 1, 1.4, 1.8 nm, which correspond to a RMS error of 0.29, 0.40, 0.52 nm respectively. The result is a set of points that are interpolated using a cubic *spline* in order to smooth the curve and avoid numerical artifacts. Note that by using spline interpolation we may get displacements between the nominal and effective maximum height, that is h/2 < |d| <= h'/2. Throughout the manuscript, we consider p = 7.5 nm. An example of the result of this process is depicted in Fig. 1d. We have implemented the 2.5D solver in a commercially available finite-element method software, Comsol Multiphysics. The geometry is created using a Matlab script in order to produce a set of points that are then interpolated directly in Comsol.

We consider coaxial nanoapertures drawn on an infinitely extended gold film of thickness H=150 nm, characterized by an internal diameter D=250 nm and a nominal gap g varying from 2 to 10 nm, as depicted in Fig. 1b-c. The structure is excited by a plane wave impinging at normal incidence through an infinite sapphire substrate. The apertures are filled with Al_2O_3 . The permittivity of sapphire is obtained using the Sellmeier's formula with parameters as in Ref. 40, while the dispersive dielectric constant of Al_2O_3 is extracted from the experimental measurements. ⁴⁹ Gold local permittivity is approximated by a Drude formula with $\hbar\omega_p=8.45$ eV and $\hbar\gamma=0.047$ eV. For completeness, we have also calculated the response of system when the electron pressure is taken into account, that is, when the metal response is nonlocal. ^{27,46,50}This is taken into account adding a correction of the form $\beta^2\nabla\nabla\cdot\mathbf{P}$ to the Drude model, ²⁷ where β is proportional to the Fermi velocity. Here we take $\beta\simeq1.3\times10^6$ m/s. In order to characterize the optical response of the systems, we compute the absorption efficiency as $q_{\rm abs}=(W_{\rm abs}-W_{\rm film})/(\sigma I_0)$, where $W_{\rm abs}$ is the power dissipated in

the entire structure, W_{film} is the power dissipated by a continuous film (i.e. without aperture), I_0 is the input intensity and $\sigma = \pi \left[(D/2 + g)^2 - (D/2)^2 \right]$ is the geometrical cross-section of the aperture. This definition removes all dependencies on the film extension.

Using the techniques described above we have generated 20 different numerical samples for each nominal gap size, for both types of gap roughness, conformal with h = 1.8 nm $(h' \simeq 2.5)$ and fully random with h = 1.4 nm $(h' \simeq 2)$. In Fig. 2, we show a set of absorption spectra around the zero-th-order mode resonance, 40,46,51 as well as the mean curve obtained by averaging the results from all the random samples. As expected, the resonance of the system undergoes a shift towards longer wavelengths as the average gap size is reduced. It is interesting to note the difference between conformal (Fig. 2a) and random (Fig. 2b) gap roughness. While in the first case (Fig. 2a) the impact of roughness is minimal, producing small oscillations of the peak resonance even for the smallest gap, in the second case (Fig. 2b), the impact of roughness is substantial and variations of the peak resonance increase as the gap size shrinks. It is clear from these simulations that the effect of the roughness is to randomly shift (towards higher or lower frequencies) the resonance of the system. An analogous behavior can be observed for other resonances (i.e. the first order Fabry-Pérot mode resonance, not reported here). In Fig. 2c, we report calculations for the same numerical samples of Fig. 2b when the nonlocal response of gold free electrons is considered. As expected the average resonance results in an increasing blue-shift compared to the local case, as the gap is reduced. More interestingly however is the fact that for each nominal gap size the spectra are more tightly packed compared to the local case. This is especially visible for smaller gaps. The effect of the electron pressure is to spread the electron accumulation charge induced by an external field inward with respect to the metal surface. This can in some cases—for example when roughness produces sub-nanometer asperities—even mitigate the detrimental impact of surface roughness on the propagation length of surface plasmons. ⁵² Analogously, in this case the effect of the electron pressure is to smooth out some roughness features so that the global effect is a reduced random oscillation of the peak resonance caused by the randomness of the roughness. Note that we set the minimum gap $g \sim 2$ nm in order to avoid quantum tunneling effects, which are not accounted for by our model. Generally quantum tunneling occurs of for gaps < 0.5 nm.

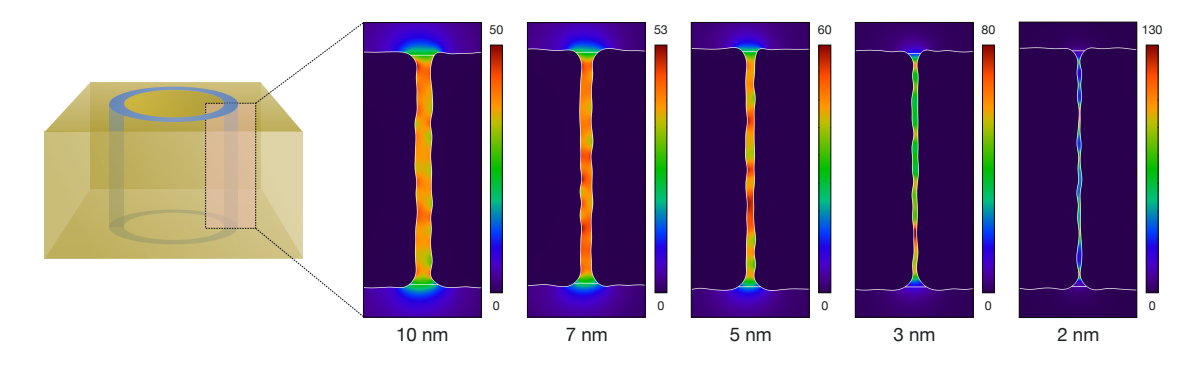


Figure 3: Field enhancement ($|\mathbf{E}|/E_0$) maps for gap sizes g=10,7,5,3,2 nm for structures with random surface roughness with h=1.4 nm ($h'\simeq 2.0$ nm). The maps are taken in correspondence of the peak resonance for each structure.

The impact of roughness on the near-field is shown in Fig. 3, where we show the electric field enhancement, $|\mathbf{E}|/E_0$, at resonance, propagating through the aperture obtained for a typical sample for each gap size. The resonance corresponds to an effective epsilon-near-zero mode, which is characterized by a constant phase, and hence norm, of the field along its propagation through the gap.⁵¹ For large gaps (> 5 nm) this is still the case, while for smaller gaps (< 3 nm) the randomness of the structure creates local hot spots where the field is strongly enhanced.

To understand the global impact of roughness on different gap sizes, in Fig. 4a we show the epsilon-near-zero mode resonance as a function of the nominal gap size g. The shaded regions represent the maximum deviation introduced by the fully random roughness. As already seen in Fig. 2, the smaller the gap the larger the variance. The mean value (indicated by triangles and squares) is mostly unchanged with respect to the perfectly smooth structure for all gaps except the smallest. In this case, the averaged resonance results are slightly shifted toward longer wavelengths compared to the smooth structure. Fig. 4a shows more clearly that the impact of electron pressure on coaxial nanoapertures is to slightly

reduce (with respect to local calculations) the shift caused by the reduction of the gap size. This is consistent with numerical results obtained for smooth structures. ⁴⁶ Together with our numerical data, we report in Fig. 4a the experimental data measured in Ref. 40. Note that the experimental data remain within the roughness deviation of the nonlocal calculations, and are clearly outside the span of local results.

It is interesting at this point to understand the nature of the shift induced by the gap roughness. In order to do so, we have evaluated the effective gap size corresponding to 3 sets of samples obtained for h = 1, 1.4, 1.8 nm ($h' \simeq 1.4, 2.0, 2.5 \text{ nm}$). The effective gap for each sample —one sample corresponds to a realization of random roughness for a given nominal gap and h— is evaluated by numerically integrating the gap surface on a vertical cross-section, see Fig. 1b, and dividing it by the gold film thickness H. The epsilon-near-zero mode resonance for each sample is plotted against the effective gap size in Fig. 4b, for both local and nonlocal cases. It is surprising how well the single samples follow the trajectory of the smooth structure. This clearly shows that the resonance shift due to roughness is mostly driven by the variation that the roughness induces in the effective gap size. It is interesting finally to note two outliers for $g \sim 2$ nm with resonances below 5 μ m. These two points are associated to the formation of conductive gaps where the roughness produces one point of contact between the two gap sides. Interestingly, in the nonlocal calculations these effects are attenuated. Such behavior however is expected to depend on the spatial extension and on the number of the points of contact. These effects are of course absent in the case of conformal roughness, where the effective gap always corresponds to the nominal gap.

In conclusion, we have analyzed the impact of nanoscale surface roughness on single coaxial nanoapertures characterized by gaps of few nanometers. Although our approach was limited to roughness on the cross-sectional plane of the systems, we are confident similar results will hold in the general case. It is very unlikely in fact that full three-dimensional surface roughness might lead to different conclusions. We have shown that while the impact of conformal gap roughness is negligible, fully random roughness might strongly affect

the resonance shift of individual samples. Moreover, the roughness-induced perturbation on the peak resonance has a strong correlation with the effective gap size for each individual sample. A large number of samples then can average out the fluctuations due to fabrication imperfections and still provide a precise measure of the ideal system's optical properties. Experimentally, this is naturally achieved by performing measurements on structure ensembles.

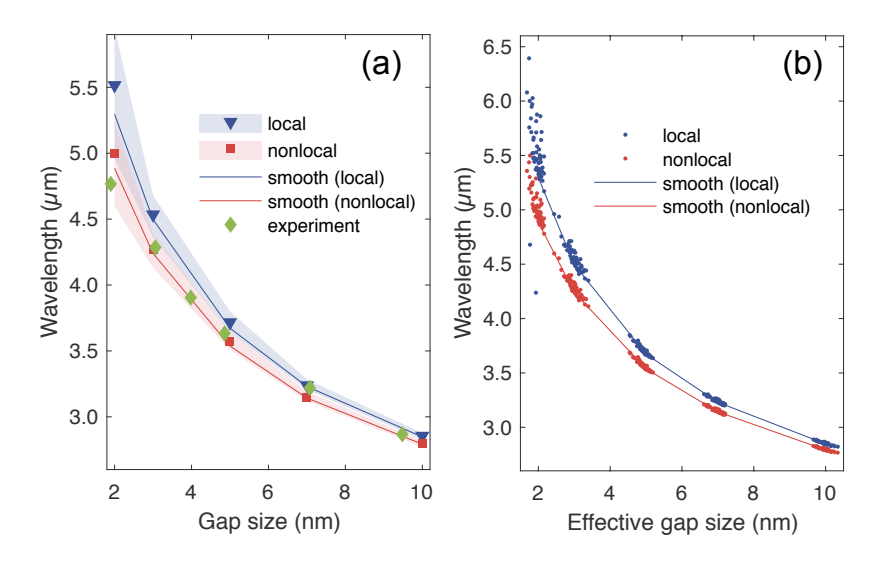


Figure 4: The resonant wavelength is tracked for the different models as a function of gap size. In (a) the shaded areas represents the maximum deviation introduced by the purely random roughness. Nonlocality (in red) always blue-shifts resonances relatively to local response calculations (in blue); the continuous lines refer to a perfectly smooth structure; experimental data from Ref. 40 are also reported. In (b) the resonance wavelength of individual structures is plotted against the effective gap size; smooth structures curves are shown for reference.

Methods

Numerical calculations are performed by solving the following system of equations in frequency domain: ^{26,27,53}

$$\nabla \times \nabla \times \mathbf{E} - \frac{\omega^2}{c^2} \mathbf{E} - \mu_0 \omega^2 \mathbf{P} = 0, \tag{1}$$

$$\beta^{2}\nabla\nabla \cdot \mathbf{P} + (\omega^{2} + i\gamma\omega)\mathbf{P} + \varepsilon_{0}\omega_{p}^{2}(\mathbf{E} + \mathbf{E}_{inc}) = 0,$$
(2)

where μ_0 and ε_0 are the permeability and permittivity of free-space, c is the speed of light in vacuum, ω_p is the plasma frequency, and β is the speed of sound in the plasma associated to the quantum pressure. **E** and **P** are the scattered electric field and the polarization vector respectively, while \mathbf{E}_{inc} is the incident field.

In order to take advantage from the symmetry of the geometry, we implemented our equations assuming an azimuthal dependence of the form $e^{-im\phi}$ with $m \in \mathbb{Z}$. That is, for a vector field \mathbf{v} , we have $\mathbf{v}(\rho, \phi, z) = \sum_{m \in \mathbb{Z}} \mathbf{v}^{(m)}(\rho, z)e^{-im\phi}$. Eqs. (2) are solved using a commercially available software based on Finite-element method (FEM). This method requires to re-write the differential problem (2) in the corresponding variational weak formulation, where some of the derivatives are distributed to the *test* functions. After integrating over ϕ , the initially three-dimensional problem is reduced into $(2m_{max} + 1)$ two-dimensional problems, characterized by the following weak form:

$$2\pi \int \left(\nabla \times \mathbf{E}^{(m)}\right) \cdot \left(\nabla \times \tilde{\mathbf{E}}^{(m)}\right) - \left(k_0^2 \mathbf{E}^{(m)} + \mu_0 \omega^2 \mathbf{P}^{(m)}\right) \cdot \tilde{\mathbf{E}}^{(m)} \rho d\rho dz = 0, \tag{3}$$

$$2\pi \int -\beta^2 \left(\nabla \cdot \mathbf{P}^{(m)}\right) \left(\nabla \cdot \tilde{\mathbf{P}}^{(m)}\right) + \left[\left(\omega^2 + i\gamma\omega\right) \mathbf{P}^{(m)} + \varepsilon_0 \omega_p^2 \left(\mathbf{E}^{(m)} + \mathbf{E}_{inc}^{(m)}\right)\right] \cdot \tilde{\mathbf{P}}^{(m)} \rho d\rho dz = 0, \tag{4}$$

where: 42,53

$$\nabla \cdot \mathbf{E}^{(m)} \equiv \left(\frac{1}{\rho} + \frac{\partial}{\partial \rho}\right) E_{\rho}^{(m)} - \frac{im}{\rho} E_{\phi}^{(m)} + \frac{\partial E_{z}^{(m)}}{\partial z}, \tag{5}$$

$$\nabla \times \mathbf{P}^{(m)} \equiv \hat{\rho} \left(-\frac{\partial P_{\phi}^{(m)}}{\partial z} - i\frac{m}{\rho} P_{z}^{(m)}\right) + \hat{\phi} \left(\frac{\partial P_{\rho}^{(m)}}{\partial z} - \frac{\partial P_{z}^{(m)}}{\partial \rho}\right) + \hat{z} \left(\frac{P_{\phi}^{(m)}}{\rho} + \frac{\partial P_{\phi}^{(m)}}{\partial \rho} + i\frac{m}{\rho} P_{\rho}^{(m)}\right), \tag{6}$$

with analogous expression for the test functions. Note that for the case of an incident plane wave propagating along the z axis, one has to solve the problem just for $m = \pm 1$. Moreover by taking into account field parities, the solution for m = 1 can be related to the solution for m = -1, so that a single two-dimensional calculation becomes necessary.^{42,53} Perfectly

matched layers have been used in order to emulate an infinite domain and avoid unwanted reflections.

Acknowledgement

F.V.-C. and J.P. acknowledge support from the AFOSR Grant No. FA9550-19-1-0240. D.Y. and S-H.O. acknowledge support from the National Science Foundation (NSF ECCS 1809723 and ECCS 1809240) and Sanford P. Bordeau Endowed Chair at the University of Minnesota. D.R.S. acknowledges funding from AFOSR (Grant No. FA9550-18-1-0187).

Notes

The authors declare no competing financial interest.

References

- Hill, R. T.; Mock, J. J.; Urzhumov, Y. A.; Sebba, D. S.; Oldenburg, S. J.; Chen, S.-Y.;
 Lazarides, A. A.; Chilkoti, A.; Smith, D. R. Leveraging nanoscale plasmonic modes to
 achieve reproducible enhancement of light. Nano Lett. 2010, 10, 4150–4154.
- Moreau, A.; Ciracì, C.; Mock, J. J.; Hill, R. T.; Wang, Q.; Wiley, B. J.; Chilkoti, A.; Smith, D. R. Controlled-reflectance surfaces with film-coupled colloidal nanoantennas. Nature 2012, 492, 86–89.
- Duan, H.; Fernández-Domínguez, A. I.; Bosman, M.; Maier, S. A.; Yang, J. K. W. Nanoplasmonics: Classical down to the nanometer scale. *Nano Lett.* 2012, 12, 1683–1689.
- 4. Chen, X.; Park, H.-R.; Pelton, M.; Piao, X.; Lindquist, N. C.; Im, H.; Kim, Y. J.; Ahn, J. S.; Ahn, K. J.; Park, N.; Kim, D.-S.; Oh, S.-H. Atomic layer lithography of wafer-

- scale nanogap arrays for extreme confinement of electromagnetic waves. *Nat. Commun.* **2013**, *4*, 2361.
- Stewart, J. W.; Akselrod, G. M.; Smith, D. R.; Mikkelsen, M. H. Toward Multispectral Imaging with Colloidal Metasurface Pixels. Adv. Mater. 2017, 29, 1602971–6.
- Chikkaraddy, R.; de Nijs, B.; Benz, F.; Barrow, S. J.; Scherman, O. A.; Rosta, E.;
 Demetriadou, A.; Fox, P.; Hess, O.; Baumberg, J. J. Single-molecule strong coupling at room temperature in plasmonic nanocavities. *Nature* 2016, 535, 127–130.
- Readman, C.; de Nijs, B.; Szabó, I.; Demetriadou, A.; Greenhalgh, R.; Durkan, C.; Rosta, E.; Scherman, O. A.; Baumberg, J. J. Anomalously Large Spectral Shifts near the Quantum Tunnelling Limit in Plasmonic Rulers with Subatomic Resolution. *Nano Lett.* 2019, 19, 2051–2058.
- 8. Halas, N. J.; Lal, S.; Chang, W.-S.; Link, S.; Nordlander, P. Plasmons in Strongly Coupled Metallic Nanostructures. *Chem. Rev.* **2011**, *111*, 3913–3961.
- Fernández-Domínguez, A. I.; Zhang, P.; Luo, Y.; Maier, S. A.; García-Vidal, F. J.;
 Pendry, J. B. Transformation-optics insight into nonlocal effects in separated nanowires.
 Phys. Rev. B 2012, 86, 241110.
- 10. Esteban, R.; Borisov, A. G.; Nordlander, P.; Aizpurua, J. Bridging quantum and classical plasmonics with a quantum-corrected model. *Nat. Comm.* **2012**, *3*, 825.
- Wiener, A.; Fernández-Domínguez, A. I.; Pendry, J. B.; Horsfield, A. P.; Maier, S. A. Nonlocal propagation and tunnelling of surface plasmons in metallic hourglass waveguides. Opt. Express 2013, 21, 27509.
- Barbry, M.; Koval, P.; Marchesin, F.; Esteban, R.; Borisov, A. G.; Aizpurua, J.; Sánchez-Portal, D. Atomistic Near-Field Nanoplasmonics: Reaching Atomic-Scale Resolution in Nanooptics. *Nano Lett.* 2015, 15, 3410–3419.

- Zhu, W.; Esteban, R.; Borisov, A. G.; Baumberg, J. J.; Nordlander, P.; Lezec, H. J.;
 Aizpurua, J.; Crozier, K. B. Quantum mechanical effects in plasmonic structures with subnanometre gaps. *Nat. Comm.* 2016, 7, 11495.
- Carnegie, C.; Griffiths, J.; de Nijs, B.; Readman, C.; Chikkaraddy, R.; Deacon, W. M.;
 Zhang, Y.; Szabó, I.; Rosta, E. R.; Aizpurua, J.; Baumberg, J. J. Room-Temperature
 Optical Picocavities below 1 nm³ Accessing Single-Atom Geometries. J. Phys. Chem.
 Lett. 2018, 9, 7146-7151.
- 15. Yang, F.; Wang, Y.-T.; Huidobro, P. A.; Pendry, J. B. Nonlocal effects in singular plasmonic metasurfaces. *Phys. Rev.* **2019**, *99*, 165423.
- 16. Baumberg, J. J.; Aizpurua, J.; Mikkelsen, M. H.; Smith, D. R. Extreme nanophotonics from ultrathin metallic gaps. *Nat. Mater.* **2019**, *18*, 668–678.
- 17. Wang, H.; Fu, K.; Drezek, R. A.; Halas, N. J. Light scattering from spherical plasmonic nanoantennas: effects of nanoscale roughness. *Appl. Phys. B* **2006**, *84*, 191–195.
- Rodríguez-Fernández, J.; Funston, A. M.; Pérez-Juste, J.; Álvarez-Puebla, R. A.; Liz-Marzán, L. M.; Mulvaney, P. The effect of surface roughness on the plasmonic response of individual sub-micron gold spheres. *Phys. Chem. Chem. Phys.* 2009, 11, 5909–5914.
- 19. Trügler, A.; Tinguely, J.-C.; Krenn, J. R.; Hohenau, A.; Hohenester, U. Influence of surface roughness on the optical properties of plasmonic nanoparticles. *Phys. Rev. B* **2011**, *83*, 916–4.
- 20. Huang, J.-S.; Callegari, V.; Geisler, P.; Brüning, C.; Kern, J.; Prangsma, J. C.; Wu, X.; Feichtner, T.; Ziegler, J.; Weinmann, P.; Kamp, M.; Forchel, A.; Biagioni, P.; Sennhauser, U.; Hecht, B. Atomically flat single-crystalline gold nanostructures for plasmonic nanocircuitry. Nat. Comm. 2010, 1, 150.

- 21. Park, J. H.; Nagpal, P.; Oh, S.-H.; Norris, D. J. Improved dielectric functions in metallic films obtained via template stripping. *Appl. Phys. Lett.* **2012**, *100*, 081105.
- 22. Martin, O. J. F.; Paulus, M. Influence of metal roughness on the near-field generated by an aperture/apertureless probe. *J. Micorsc.* **2002**, *205*, 147–152.
- 23. Tinguely, J.-C.; Sow, I.; Leiner, C.; Grand, J.; Hohenau, A.; Felidj, N.; Aubard, J.; Krenn, J. R. Gold Nanoparticles for Plasmonic Biosensing: The Role of Metal Crystallinity and Nanoscale Roughness. *BioNanoSci.* 2011, 1, 128–135.
- 24. Lumdee, C.; Yun, B.; Kik, P. G. Effect of surface roughness on substrate-tuned gold nanoparticle gap plasmon resonances. *Nanoscale* **2015**, *7*, 4250–4255.
- 25. Ning, T.; Gao, S.; Huo, Y.; Jiang, S.; Yang, C.; Li, J.; Zhao, Y.; Man, B. Third-harmonic generation from gold nanowires of rough surface considering classical nonlocal effect. *Opt. Express* **2017**, *25*, 6372–11.
- Ciracì, C.; Hill, R. T.; Mock, J. J.; Urzhumov, Y. A.; Fernandez-Dominguez, A. I.;
 Maier, S. A.; Pendry, J. B.; Chilkoti, A.; Smith, D. R. Probing the ultimate limits of plasmonic enhancement. Science 2012, 337, 1072–1074.
- 27. Raza, S.; Bozhevolnyi, S. I.; Wubs, M.; Mortensen, N. A. Nonlocal optical response in metallic nanostructures. *J. Phys.: Condens. Mat.* **2015**, *27*, 183204.
- 28. Doyle, D.; Charipar, N.; Argyropoulos, C.; Trammell, S. A.; Nita, R.; Naciri, J.; Piqué, A.; Herzog, J. B.; Fontana, J. Tunable Subnanometer Gap Plasmonic Metasurfaces. ACS Photonics 2017, 5, 1012–1018.
- 29. Hajisalem, G.; Min, Q.; Gelfand, R.; Gordon, R. Effect of surface roughness on self-assembled monolayer plasmonic ruler in nonlocal regime. *Opt. Express* **2014**, *22*, 9604.
- 30. Hajisalem, G.; Nezami, M. S.; Gordon, R. Probing the quantum tunneling limit of plasmonic enhancement by third harmonic generation. *Nano Lett.* **2014**, *14*, 6651–6654.

- 31. Ciracì, C.; Chen, X.; Mock, J. J.; McGuire, F.; Liu, X.; Oh, S.-H.; Smith, D. R. Film-coupled nanoparticles by atomic layer deposition: Comparison with organic spacing layers. *Appl. Phys. Lett.* **2014**, *104*, 023109.
- 32. Kern, J.; Großmann, S.; Tarakina, N. V.; Häckel, T.; Emmerling, M.; Kamp, M.; Huang, J.-S.; Biagioni, P.; Prangsma, J. C.; Hecht, B. Atomic-scale confinement of resonant optical fields. *Nano Lett.* **2012**, *12*, 5504–5509.
- 33. Savage, K. J.; Hawkeye, M. M.; Esteban, R.; Borisov, A. G.; Aizpurua, J.; Baumberg, J. J. Revealing the quantum regime in tunnelling plasmonics. *Nature* **2012**, *491*, 574–577.
- 34. Scholl, J. A.; García-Etxarri, A.; Koh, A. L.; Dionne, J. A. Observation of quantum tunneling between two plasmonic nanoparticles. *Nano Lett.* **2013**, *13*, 564–569.
- 35. Raza, S.; Stenger, N.; Stenger, N.; Kadkhodazadeh, S.; Kadkhodazadeh, S.; Fischer, S. V.; Fischer, S. V.; Kostesha, N.; Jauho, A.-P.; Burrows, A.; Wubs, M.; Mortensen, N. A. Blueshift of the surface plasmon resonance in silver nanoparticles studied with EELS. *Nanophotonics* **2013**, *2*, 131–138.
- 36. Cha, H.; Yoon, J. H.; Yoon, S. Probing Quantum Plasmon Coupling Using Gold Nanoparticle Dimers with Tunable Interparticle Distances Down to the Subnanometer Range. ACS Nano 2014, 8, 8554–8563.
- 37. Tan, S. F.; Wu, L.; Yang, J.; Bai, P.; Bosman, M.; 2014, Quantum plasmon resonances controlled by molecular tunnel junctions. *Science* **2014**, *343*, 1496–1499.
- 38. Zhu, W.; Crozier, K. B. Quantum mechanical limit to plasmonic enhancement as observed by surface-enhanced Raman scattering. *Nat. Commun.* **2014**, *5*, 5228.
- 39. Campos, A.; Troc, N.; Cottancin, E.; Pellarin, M.; Weissker, H.-C.; Lermé, J.; Ko-

- ciak, M.; Hillenkamp, M. Plasmonic quantum size effects in silver nanoparticles are dominated by interfaces and local environments. *Nat. Physics* **2019**, *15*, 275–280.
- Yoo, D.; Vidal-Codina, F.; Ciracì, C.; Nguyen, N.-C.; Smith, D. R.; Peraire, J.; Oh, S.-H. Modeling and observation of mid-infrared nonlocality in effective epsilon-near-zero ultranarrow coaxial apertures. *Nat. Comm.* 2019, 40, 4476.
- 41. Kretschmann, E.; Ferrell, T. L.; Ashley, J. C. Splitting of the dispersion relation of surface plasmons on a rough surface. *Phys. Rev. Lett.* **1979**, *42*, 1312–1314.
- 42. Ciracì, C.; Smith, D. R.; Urzhumov, Y. A. Far-field analysis of axially symmetric three-dimensional directional cloaks. *Opt. Express* **2013**, *21*, 9397–9406.
- 43. Jurga, R.; D'Agostino, S.; Della Sala, F.; Ciracì, C. Plasmonic Nonlocal Response Effects on Dipole Decay Dynamics in the Weak- and Strong-Coupling Regimes. *J. Phys. Chem. C* **2017**, *121*, 22361–22368.
- 44. Schmitt, N.; Scheid, C.; Viquerat, J.; Lanteri, S. Simulation of three-dimensional nanoscale light interaction with spatially dispersive metals using a high order curvilinear DGTD method. *J. Comput. Phys.* **2018**, *373*, 210–229.
- 45. Li, L.; Lanteri, S.; Mortensen, N. A.; Wubs, M. A hybridizable discontinuous Galerkin method for solving nonlocal optical response models. *Comput. Phys. Commun.* **2017**, 219, 99–107.
- 46. Vidal-Codina, F.; Nguyen, N. C.; Oh, S. H.; Peraire, J. A hybridizable discontinuous Galerkin method for computing nonlocal electromagnetic effects in three-dimensional metallic nanostructures. *J. Comput. Phys.* **2018**, *355*, 548–565.
- 47. Nagpal, P.; Lindquist, N. C.; Oh, S. H.; Norris, D. J. Ultrasmooth Patterned Metals for Plasmonics and Metamaterials. *Science* **2009**, *325*, 594–597.

- 48. Zayats, A. V.; Smolyaninov, I. I.; Maradudin, A. A. Nano-optics of surface plasmon polaritons. *Physics Reports* **2005**, *408*, 131–314.
- 49. Kischkat, J.; Peters, S.; Gruska, B.; Semtsiv, M.; Chashnikova, M.; Klinkmüller, M.; Fedosenko, O.; MacHulik, S.; Aleksandrova, A.; Monastyrskyi, G.; Flores, Y.; Masselink, W. T. Mid-infrared optical properties of thin films of aluminum oxide, titanium dioxide, silicon dioxide, aluminum nitride, and silicon nitride. Appl. Optics 2012, 51, 6789–6798.
- 50. Shen, H.; Chen, L.; Ferrari, L.; Lin, M.-H.; Mortensen, N. A.; Gwo, S.; Liu, Z. Optical Observation of Plasmonic Nonlocal Effects in a 2D Superlattice of Ultrasmall Gold Nanoparticles. *Nano Lett.* **2017**, *17*, 2234–2239.
- 51. Yoo, D.; Nguyen, N.-C.; Martín Moreno, L.; Mohr, D. A.; Carretero-Palacios, S.; Shaver, J.; Peraire, J.; Ebbesen, T. W.; Oh, S.-H. High-Throughput Fabrication of Resonant Metamaterials with Ultrasmall Coaxial Apertures via Atomic Layer Lithography. *Nano Lett.* **2016**, *16*, 2040–2046.
- 52. Wiener, A.; Fernández-Domínguez, A. I.; Horsfield, A. P.; Pendry, J. B.; Maier, S. A. Nonlocal effects in the nanofocusing performance of plasmonic tips. *Nano Lett.* 2012, 12, 3308–3314.
- 53. Ciracì, C.; Smith, D. R.; Urzhumov, Y. A. Effects of classical nonlocality on the optical response of three-dimensional plasmonic nanodimers. *J. Opt. Soc. Am. B* **2013**, *30*, 2731–2736.

Graphical TOC Entry

